

The Curious Case of a Phenylated Guanidinoquinoline Ligand: Synthesis, Complexes and ATRP Properties of DMEG6phqu

Thomas Rösener,^[a] Konstantin Kröckert,^[a] Alexander Hoffmann,^[a] and Sonja Herres-Pawlis^{*[a]}

Dedicated to Professor Werner Uhl on the Occasion of his 65th Birthday

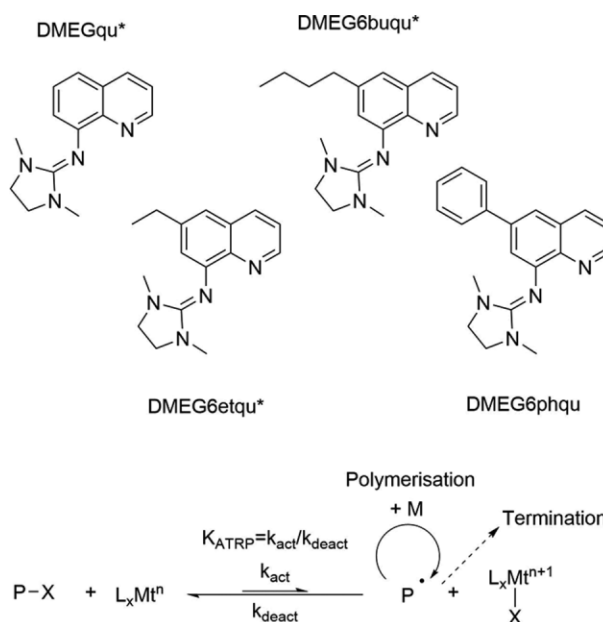
Abstract. In previous studies, copper halide complexes of the guanidinoquinoline (GUAqu) ligands 1,3-dimethyl-*N*-(quinolin-8-yl)-imidazolidin-2-imine (DMEGqu) and 1,1,3,3-tetramethyl-2-(quinolin-8-yl)-guanidine (TMGqu) were successfully implemented in atom transfer radical polymerization (ATRP) and could be further enhanced by introduction of alkyl substituents at C6 position of the quinoline backbone. Herein, the ligand DMEG6phqu is presented. The quinoline backbone of this ligand is equipped with a phenyl substituent at C6 position. This study deals with the influence of the phenyl substituent on solubility and molecular structural properties of DMEG6phqu Cu^I

and Cu^{II} bromide complexes. In contrast to previously reported systems, the Cu^IBr complex of DMEG6phqu crystallizes as a trigonal coordinated monochelate complex. However, NMR and UV/Vis spectroscopic experiments indicate that DMEG6phqu forms a bischelate species in solution. The influence of the substituent on the complex redox potential and ATRP equilibrium constant K_{ATRP} is discussed. In contrast to expectations, it turned out that copper halide complexes of DMEG6phqu are completely insoluble in the apolar monomer styrene. However, ATRP kinetics were performed in solution and the results are compared to previous studies.

Introduction

Atom transfer radical polymerization (ATRP) was invented by several independent groups in 1995 and rapidly became one of the most versatile reversible-deactivation radical polymerization (RDRP) methods.^[1] In ATRP transition metal complexes mediate an equilibrium between dormant and active radical species (Scheme 1). The complex on the left side of the equilibrium (L_xM^{n+1}) is often referred to as the activator complex, whereas its counterpart on the other side of the equilibrium ($L_xM^{n+1}-X$) is named deactivator complex. Because of the ATRP equilibrium, only few active radical species coexist and thus, chain termination reactions can be effectively suppressed. In the past, a large variety of RDRP techniques based on ATRP was developed. These allow the application of air-stable catalyst precursors, the drastic reduction of transition metal concentration and an even higher controllability.^[4] Amongst other factors, the polymerization rate in ATRP highly depends on the nature of the chosen catalyst. Catalytic properties of the transition metal complex can be easily adjusted by the ligand environment. In copper ATRP a large variety of different N-donor ligands has been evaluated and structure-reactivity-relationships were derived. The activity of a copper complex in ATRP is influenced by the denticity of the ligand, nature of the N-donor and its electron donating ability.^[5] Stud-

ies of different 4,4'-substituted 2,2'-bipyridine ligands gained further insights into the influence of ligand substitution on catalyst activities.^[6] Decoration of pyridine based ligands with electron donating substituents had by far the largest influence on catalyst activity and thus, the most active ATRP catalyst features the tetrapodal ligand TMPA^{NMe2}.^[7]



Scheme 1. The ATRP equilibrium and various DMEGqu-based ligands. Ligands marked with an asterisk were already presented in previous publications.^[2,3]

In the past, our focus lay on the implementation of guanidino ligands as a new and promising ligand class in ATRP.

* Prof. Dr. S. Herres-Pawlis
E-Mail: sonja.herres-pawlis@ac.rwth-aachen.de

[a] Institut für Anorganische Chemie
RWTH Aachen University
Landoltweg 1
52074 Aachen, Germany

Supporting information for this article is available on the WWW under <http://dx.doi.org/10.1002/zaac.201800258> or from the author.

Guanidines represent a class of strong and neutral N-donors and they have great potential in ATRP. Guanidine ligands already found broad application in the field of homogeneous catalysis. Recent publications describe the application in the ring opening polymerization (ROP) of lactide^[8] or oxygen activation.^[9] However, only few examples of guanidine complexes in ATRP are known.^[10] In a previous publication we showed that copper complexes of the bidentate guanidinoquinoline (GUAqu) ligands 1,3-dimethyl-*N*-(quinolin-8-yl)-imidazolidin-2-imine (DMEGqu) and 1,1,3,3-tetramethyl-2-(quinolin-8-yl)-guanidine (TMGqu) successfully can mediate ATRP reactions (Scheme 1).^[2] These ligands also attracted attention in the fields of copper photochemistry^[11] and as entatic state models for electron transfer proteins.^[12,13]

The introduction of alkyl substituents led to better solubility of the complexes in styrene and thus better control of the polymerization reaction. It is also worth mentioning that alkylated versions of DMEGqu showed almost no differences in electronic properties in comparison with the parental ligand.^[3]

In this publication, the ligand DMEG6phqu is presented. The quinoline backbone of this ligand is equipped with a phenyl substituent at C6 position. A synthetic strategy for the synthesis of C6 phenylated GUA6Phqu ligands is presented. Cu^I and Cu^{II} bromide complexes of DMEG6phqu were investigated with respect to their structural characteristics, since they represent activator and deactivator complexes in an ATRP. The focus of this work lay on solubility of corresponding complexes in the monomer and the influence of the phenyl substituent on electronic and ATRP properties of these complexes.

Results and Discussion

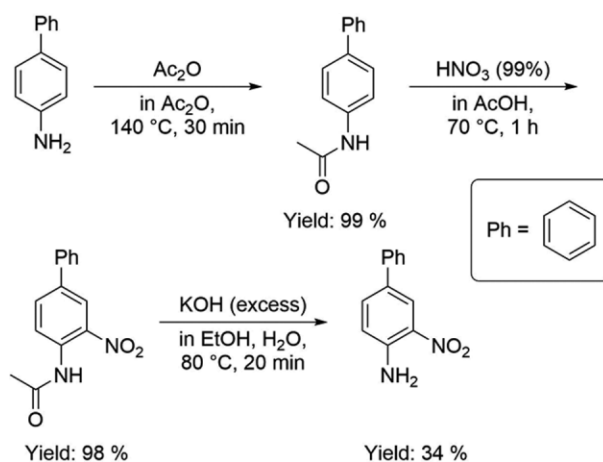
Synthesis of GUA6phqu Ligands

First, attempts were made to synthesize GUA6phqu ligands following a published protocol.^[3] With this method, a large variety of C6 substituted guanidinoquinoline ligands can be synthesized starting from 4-substituted anilines. For the synthesis of GUA6phqu ligands, 4-aminobiphenyl was used as starting material. It appeared that 4-aminobiphenyl is insoluble in various organic solvents rendering the original nitration step impossible. Hence, the nitration step had to be modified. Following slightly modified literature protocols,^[14–16] the synthesis of 3-nitro-4-aminobiphenyl (NO₂phan) could be accomplished. An overview of the synthetic steps is shown in Scheme 2.

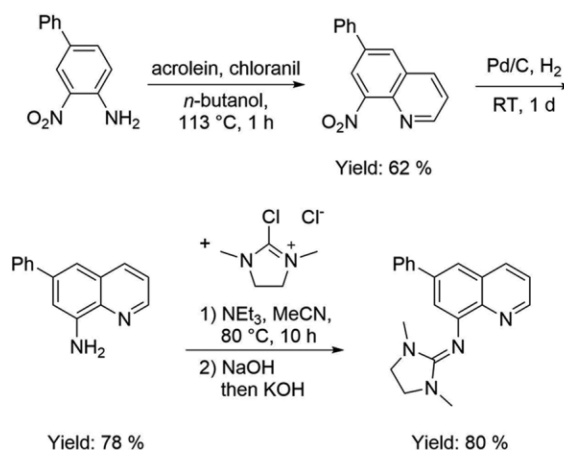
In contrast to the previously published synthetic strategy, the intermediates here had to be isolated. Crude NO₂phan was purified by recrystallization from ethanol, which went hand in hand with a significant loss of yield but resulted in pure product. Consequently, the purification step must be improved with respect to product yield in follow-up studies.

Subsequently, NO₂phan was stepwise reacted to 6-phenylquinolin-8-amine (NH₂6phqu), following the synthetic strategy previously published.^[3] An overview of the synthetic steps is shown in Scheme 3.

The ligand precursor was reacted with DMEG Vilsmeier salt to provide DMEG6phqu following a common procedure.^[17,18]



Scheme 2. Synthesis of NO₂phan: modified nitration step for the synthesis of GUA6phqu.



Scheme 3. Synthesis of DMEG6phqu starting from NO₂phan, following a previously published synthetic strategy.^[3]

DMEG6phqu was purified via recrystallization from acetonitrile. Thus, crystals suitable for X-ray crystallography were obtained. In Table 1 key structural parameters of DMEG6phqu as well as of DMEGqu and DMEG6etqu are summarized. Key bond lengths within the ligand are not significantly altered by substitution at the C6 position.

Table 1. Selected bond lengths /Å and ρ of DMEG6phqu in comparison with DMEGqu^[19] and DMEG6etqu.^[3]

	DMEG6phqu	DMEGqu (Parent ligand)	DMEG6etqu
C ₈ –N _{GUA}	1.391(2)	1.394(2)	1.384(2)
C _{GUA} –N _{GUA}	1.291(2)	1.283(3)	1.291(2)
C _{GUA} –N _{Amine}	1.380(av)	1.381(av)	1.360(av)
C _{8a} –N _{qu}	1.372(2)	1.371(2)	1.364(2)
Geometrical factor ρ ^{a)}	0.94	0.93	0.95

a) $\rho = 2a/(b + c)$ with $a = d(\text{C}_{\text{GUA}}\text{--N}_{\text{GUA}})$ and b and $c = d(\text{C}_{\text{GUA}}\text{--N}_{\text{amine}})$.^[20]

Copper Halide Complexes of DMEG6phqu

Structural Characterization in Solid State

Reaction of DMEG6phqu with anhydrous $\text{Cu}^{\text{I}}\text{Br}$ and $\text{Cu}^{\text{II}}\text{Br}_2$ in acetonitrile resulted in complex solutions of dark red color.

Bright orange crystals of the monochelate complex $[\text{Cu}(\text{DMEG6phqu})\text{Br}]$ were crystallized from the Cu^{I} solution. The central metal is coordinated by one bidentate DMEG6phqu ligand and an additional bromido ligand in a trigonal planar fashion. In contrast to the $\text{Cu}^{\text{I}}\text{Br}$ complex of DMEG6phqu, analogous complexes of the ligands DMEGqu and DMEG6etqu could be crystallized as bischelates, where two bidentate DMEG6Rqu ($R = \text{H}, \text{et}$) ligands are coordinated.^[2,3] The molecular structure of the complex is depicted in Figure 1 and key structural parameters are summarized in Table 2.

Comparing $\text{Cu}-\text{N}_{\text{GUA}}$ and $\text{Cu}-\text{N}_{\text{qu}}$ bond lengths, it appears that the former is significantly shortened [2.045(2) Å] and the latter is significantly prolonged [2.015(2) Å] in comparison with bischelate DMEG6Rqu ($R = \text{H}, \text{et}$) complexes (typically around 2.10 Å for $\text{Cu}-\text{N}_{\text{GUA}}$ or 1.97 Å for $\text{Cu}-\text{N}_{\text{qu}}$). As already stated in a previous publication,^[2] due to the rigid aromatic backbone of GUAqu ligands, shortening of $\text{Cu}-\text{N}_{\text{GUA}}$ goes hand in hand with elongation of $\text{Cu}-\text{N}_{\text{qu}}$ and vice versa. The exceptional short $\text{Cu}-\text{N}_{\text{GUA}}$ bond length can be drawn back to the absence of a second coordinating DMEG6phqu ligand. The ρ value is a measure for the delocalization within the guanidine moiety.^[20] Strong coordination of N_{GUA} is affiliated with enhanced delocalization of electron density within the guanidine moiety. In the complex $[\text{Cu}(\text{DMEG6phqu})\text{Br}]$, ρ is nearly 1 due to the strong coordination of the sole guanidine function. In contrast to that, in bischelate Cu^{I} complexes of DMEGqu and DMEG6etqu, the ρ value is smaller (typically around 0.97). Bond angles within the coordination sphere are

Table 2. Key bond lengths /Å and angles /° of the Cu^{I} complex $[\text{Cu}(\text{DMEG6phqu})\text{Br}]$ and the Cu^{II} complex $[\text{Cu}(\text{DMEG6phqu})_2\text{Br}]$.

	$[\text{Cu}(\text{DMEG6phqu})\text{Br}]$	$[\text{Cu}(\text{DMEG6phqu})_2\text{Br}]\text{Br}$
Bond length		
Cu–Br	2.2641(5)	2.5082(6)
Cu– $\text{N}_{\text{GUA}}(1)$	2.045(2)	2.075(3)
Cu– $\text{N}_{\text{GUA}}(2)$	–	2.131(3)
Cu– $\text{N}_{\text{qu}}(1)$	2.015(2)	1.972(3)
Cu– $\text{N}_{\text{qu}}(2)$	–	1.980(3)
Bond angle		
$\text{N}_{\text{GUA}}(1)-\text{Cu}-\text{N}_{\text{GUA}}(2)$	–	115.3(1)
$\text{N}_{\text{GUA}}(1)-\text{Cu}-\text{N}_{\text{qu}}(1)$	82.2(1)	80.8(1)
$\text{N}_{\text{GUA}}(2)-\text{Cu}-\text{N}_{\text{qu}}(2)$	–	80.9(1)
$\text{N}_{\text{GUA}}(1)-\text{Cu}-\text{X}$	136.6(1)	134.9(1)
$\text{N}_{\text{qu}}(1)-\text{Cu}-\text{N}_{\text{qu}}(2)$	–	176.0(1)
$\text{N}_{\text{qu}}(1)-\text{Cu}-\text{X}$	141.2(1)	91.7(1)
Geometrical factor		
τ_5^{a}	–	0.69
ρ^{b}	0.99	1.00

a) $\tau_5 = \frac{\alpha - \beta}{60}$,^[21] b) $\rho = 2a/(b + c)$ with $a = d(\text{C}_{\text{GUA}}-\text{N}_{\text{GUA}})$ and $b = c = d(\text{C}_{\text{GUA}}-\text{N}_{\text{amine}})$.^[20] Average ρ value of both guanidine moieties in the case of the bischelate complex.

mainly determined by the ligand bite angle of 82.2(1)°. Thus, $\text{N}_{\text{GUA}}(1)-\text{Cu}-\text{X}$ and $\text{N}_{\text{qu}}(1)-\text{Cu}-\text{X}$ are found at ca. 140°.

The $\text{Cu}^{\text{II}}\text{Br}_2$ complex consists of two coordinating bidentate ligands and an additional coordinating bromido ligand. The coordination sphere resembles a distorted trigonal bipyramid. Considering bond lengths, it can be noticed that $[\text{Cu}(\text{DMEG6phqu})_2\text{Br}]\text{Br}$ does not significantly differ from previously published complexes with the ligands DMEGqu and DMEG6etqu. ρ and τ_5 values of $[\text{Cu}(\text{DMEG6phqu})_2\text{Br}]\text{Br}$ also resemble those of $\text{Cu}^{\text{II}}\text{Br}_2$ complexes of DMEGqu and DMEG6etqu.

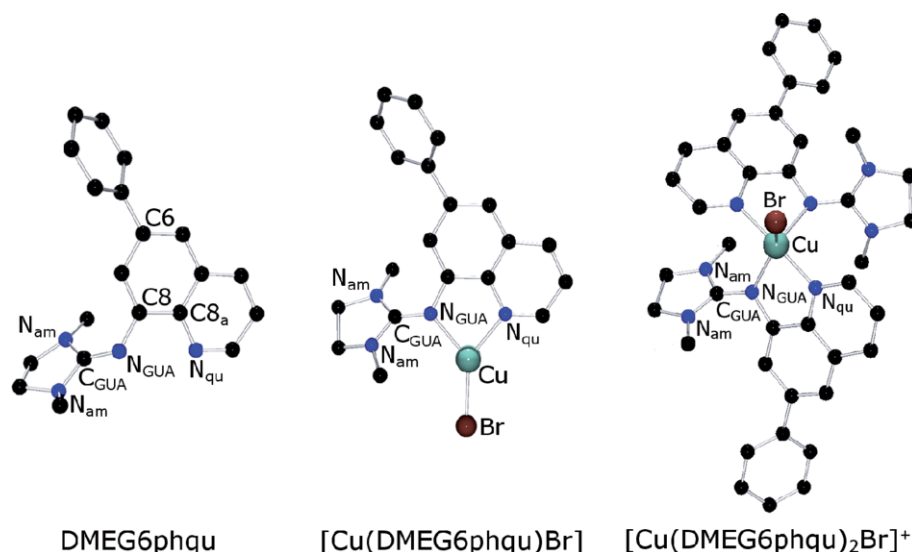


Figure 1. Molecular structures of DMEG6phqu, $[\text{Cu}(\text{DMEG6phqu})\text{Br}]$, and the complex cation of $[\text{Cu}(\text{DMEG6phqu})_2\text{Br}]\text{Br}$ in the solid state. Key atoms are exemplarily marked. Hydrogen atoms are omitted for clarity.

Structural Characterization in Solution

It appeared that complex solutions of DMEG6phqu with $\text{Cu}^{\text{I}}\text{Br}$ were of different color than corresponding crystals (dark red vs. bright orange). This indicates that the complex might have different structures in solution and solid state. For the characterization of the $\text{Cu}^{\text{I}}\text{Br}$ activator complex in solution, NMR and mass spectrometry experiments were performed. Additionally, a UV/Vis titration experiment was conducted. For the NMR experiment, the complex was generated in situ by reacting DMEG6phqu with $\text{Cu}^{\text{I}}\text{Br}$ in a ratio of 2:1 in $[\text{D}_3]\text{MeCN}$. This solution was subjected to NMR spectroscopy and mass spectrometry. The NMR spectra are depicted in Figures S13 and S14 (Supporting Information). Within the NMR timescale, one set of NMR signals could be measured. The absence of a second set of NMR signals indicates, that a bischelate complex $[\text{Cu}(\text{DMEG6phqu})_2]\text{Br}$ is formed. Narrow NMR signals indicate that the solution was free of Cu^{II} . To rule out a possible fast exchange of different Cu^{I} species variable temperature NMR spectroscopy was conducted. Here, DMEG6phqu and $\text{Cu}^{\text{I}}\text{Br}$ were also used in a molar ratio of 2:1. The VT-NMR spectra are depicted in Figures S15 and S16 (Supporting Information). A temperature range from $-40\text{ }^\circ\text{C}$ to $+40\text{ }^\circ\text{C}$ was investigated. Upon decreasing the temperature, the peaks associated with the DMEG moieties within the complex resolve due to the slower motion of these groups. Fast equilibria between different Cu^{I} species and free and associated ligand could not be proven. In HR mass spectra also the bischelate complex was found (see data in the Experimental Section). In an additional experiment, a solution of CuBr in MeCN was titrated with DMEG6phqu. Formation of $[\text{Cu}(\text{DMEG6phqu})_2]\text{Br}$ was followed by UV/Vis spectroscopy. In Figure 2, the UV/Vis spectrum of $[\text{Cu}(\text{DMEG6phqu})_2]\text{Br}$ is depicted.

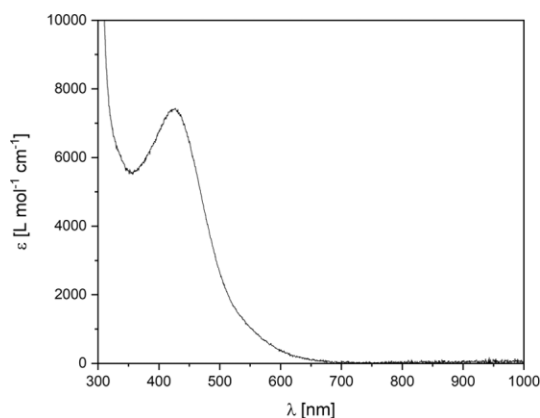


Figure 2. UV/Vis spectrum of $[\text{Cu}(\text{DMEG6phqu})_2]\text{Br}$ ($1.1 \times 10^{-3}\text{ mol}\cdot\text{L}^{-1}$ in MeCN).

$[\text{Cu}(\text{DMEG6phqu})_2]\text{Br}$ possesses an absorption at ca. 430 nm ($\epsilon = 7300\text{ L}\cdot\text{mol}^{-1}\cdot\text{cm}^{-1}$) that is associated with a metal-to-ligand charge transfer (MLCT) which could be also found in bischelate Cu^{I} complexes of DMEGqu and TMGqu.^[12] However, the absorption maximum of DMEGqu and TMGqu complexes lies at 445 nm. The absence of a typi-

cal d–d transition at 945 nm indicates furthermore that the solution was free of the Cu^{II} species $[\text{Cu}(\text{DMEG6phqu})_2]\text{Br}$. The absorption was followed when titrating a solution of $\text{Cu}^{\text{I}}\text{Br}$ with the ligand. Figure 3 shows the corresponding titration curve.

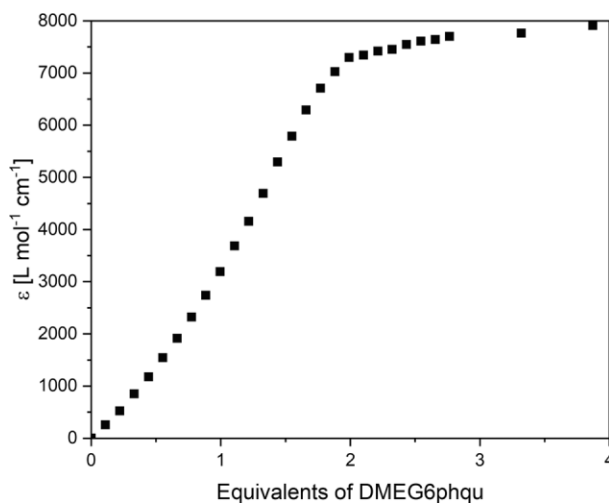


Figure 3. Titration of $\text{Cu}^{\text{I}}\text{Br}$ ($1.8 \times 10^{-3}\text{ mol}\cdot\text{L}^{-1}$ in MeCN) with DMEG6phqu. Absorption trace at 430 nm.

The absorption at 430 nm increases with addition of ligand. After addition of two equivalents of ligand the absorption trace begins to flatten, but however, does not reach its maximum. With addition of excess ligand, an absorption at 350 nm that is associated with free ligand, starts to increase. The titration curve is slightly influenced by this ligand-associated absorption band. Figure S3 (Supporting Information) shows the UV/Vis spectrum of $[\text{Cu}(\text{DMEG6phqu})_2]\text{Br}$ after addition of excess ligand. The titration experiment indicates that a bischelate complex is formed. After addition of two equivalents of ligand, all the Cu^{I} is coordinated by two ligands and the absorption trace flattens.

In the case of the paramagnetic Cu^{II} deactivator complex $[\text{Cu}(\text{DMEG6phqu})_2]\text{Br}$, EPR spectroscopy was used for the structural characterization of the complex in solution.

EPR spectra of $[\text{Cu}(\text{DMEG6phqu})_2]\text{Br}$ were measured both in solid state and in MeCN at room temperature. Both spectra show significant broadening (see Figure S1, Supporting Information) that is caused by a strong electron delocalization between the guanidine donors and the bromido ligand.^[22] Since $[\text{Cu}(\text{DMEG6phqu})_2]\text{Br}$ shows low solubility in MeCN, the solution EPR spectrum appears to be noisy. Both spectra resemble each other which indicates that $[\text{Cu}(\text{DMEG6phqu})_2]\text{Br}$ exists as a pentacoordinate complex both in solid state and in solution.

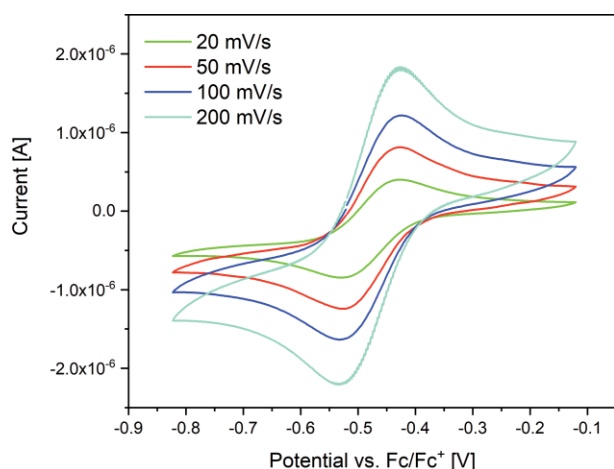
Electrochemistry

Matyjaszewski et al. found a linear correlation between the redox potential of a complex in solution and its activity in ATRP.^[23] Since electrochemical properties provide information about the catalyst activities, cyclic voltammetry was

Table 3. $E_{1/2}$ for $\text{Cu}^{\text{II}}\text{Br}_2$ complexes with DMEG6phqu, DMEGqu, DMEG6etqu, and DMEG6buqu[3] (potential vs. Fc/Fc⁺ and SCE^[24]).

Complex	$E_{1/2}$ vs. Fc/Fc ⁺ /mV	$E_{1/2}$ vs. SCE /mV	ΔE_p /mV
[Cu(DMEG6phqu) ₂ Br]Br	-480 ± 5	-80 ± 5	85 ± 5
[Cu(DMEGqu) ₂ Br]Br	-480 ± 5	-80 ± 5	85 ± 5
[Cu(DMEG6etqu) ₂ Br]Br	-465 ± 5	-65 ± 5	80 ± 5
[Cu(DMEG6buqu) ₂ Br]Br	-480 ± 5	-80 ± 5	85 ± 5

performed in acetonitrile starting from crystalline complex [Cu(DMEG6phqu)₂Br]Br. All measurements were carried out at room temperature at different scan rates to prove reversible behavior of the redox process. $E_{1/2}$ was determined against the Fc/Fc⁺ couple and for better comparability with literature data, recalculated against SCE.^[24] Figure 4 shows cyclic voltammograms of the [Cu^I(DMEG6phqu)₂Br]/[Cu^{II}(DMEG6phqu)₂Br]⁺ couple at different scan rates.

**Figure 4.** Cyclic voltammograms of the [Cu(DMEG6phqu)₂Br]/[Cu(DMEG6phqu)₂Br]⁺ couple at different scan rates starting from [Cu(DMEG6phqu)₂Br]Br.

$E_{1/2}$ values of [Cu(DMEG6phqu)₂Br]Br and the $\text{Cu}^{\text{II}}\text{Br}_2$ complexes of DMEG6Rqu ($R = \text{H, et, bu}$) are listed in Table 3.

The introduction of an electron withdrawing phenyl substituent at C6 position of the quinoline backbone of the DMEG6Rqu ligand does not significantly change the redox potential of corresponding complexes. As already demonstrated for Cu complexes of alkylated DMEG6Rqu ligands, substitution has almost no effect on the donor properties of this class of ligands. Based on the CV data, it is predicted that [Cu(DMEG6phqu)₂Br] resembles complexes of unsubstituted DMEGqu and alkylated DMEG6etqu and DMEG6buqu in their activity in ATRP.

Atom Transfer Radical Polymerization

Determination of K_{ATRP}

K_{ATRP} is the central equilibrium constant of the ATRP equilibrium (see Scheme 1) and represents the ratio of the rate con-

stants of activation k_{act} and deactivation k_{deact} . Polymerization velocity and control highly depend on K_{ATRP} .

Herein, K_{ATRP} was determined by reacting the [Cu^I(DMEG6phqu)₂]Br activator complex with an ATRP initiator and following the evolution of the [Cu^{II}(DMEG6phqu)₂Br]Br deactivator species via UV/Vis spectroscopy (details of the procedure can be found in the Experimental Section). The activator complex was generated in situ by reacting DMEG6phqu with Cu^IBr in a ratio of 2/1. As discussed earlier, thus the bischelate complex [Cu(DMEG6phqu)₂]Br is formed.

To follow the formation of the Cu^{II} complex, a characteristic d-d transition band in the area around 900-950 nm was chosen. The maximum of this absorption lies at 945 nm and the extinction coefficient ϵ was determined to 360 L·mol⁻¹·cm⁻¹.

K_{ATRP} of [Cu(DMEG6phqu)₂]Br was determined at 22 °C in acetonitrile with ethyl α -bromoisobutyrate (EBrib) as initiator and calculated by the method developed by *Matyjaszewski*.^[25] One exemplary plot of F(Y) vs. time is shown in Figure S2 (Supporting Information). K_{ATRP} values for [Cu(DMEG6phqu)₂]Br and the analogous Cu^IBr complexes of DMEGqu, DMEG6etqu, and DMEG6buqu are summarized in Table 4.

Table 4. K_{ATRP} values for [Cu(L)₂]Br (L = DMEG6phqu, DMEGqu, DMEG6etqu, and DMEG6buqu).^[3]

[Cu(L) ₂]Br; L =	K_{ATRP} (<i>Matyjaszewski</i>)
DMEG6phqu	$7.4 \pm 0.9 \times 10^{-08}$
DMEGqu	$9.0 \pm 0.7 \times 10^{-08}$
DMEG6etqu	$7.9 \pm 0.1 \times 10^{-08}$
DMEG6buqu	$7.8 \pm 0.7 \times 10^{-08}$

In Figure 5 the logarithmic values of K_{ATRP} (calculated via the method of *Matyjaszewski*) are plotted against $E_{1/2}$ determined via CV. All values roughly follow the correlation published by *Matyjaszewski* et al.^[23]

The introduction of a phenyl substituent at C6 position of the quinoline backbone has no significant influence on the electronic/donor properties of the resulting ligand. This is also expressed in a K_{ATRP} that is not significantly altered in comparison with other DMEG6Rqu ($R = \text{H, et, bu}$) ligands.

Complexes of the bidentate DMEG6Rqu ($R = \text{H, et, bu, or ph}$) ligands exhibit redox potentials and values for K_{ATRP} comparable to complexes of the tridentate ligand PMDETA. It must be mentioned, that PMDETA forms complexes with three participating N-donors, whereas DMEG6Rqu forms bischelate complexes with four participating N-donors.

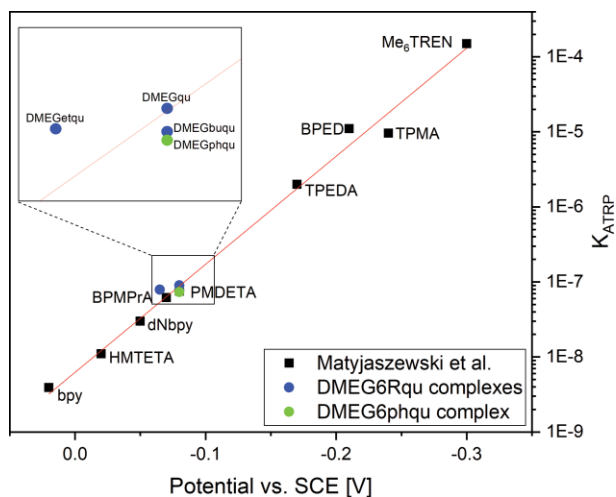


Figure 5. Correlation of $\text{Cu}^{\text{I}}/\text{L}$ redox potentials with K_{ATRP} values (measured with EBrib at 22 °C in MeCN). Black squares: Values published by Matyjaszewski et al.^[23] Blue circles: Values for DMEG6Rqu complexes previously published.^[3] Green circles: Value for the DMEG6phqu complex.

Polymerization Kinetics

Although it was expected that $[\text{Cu}(\text{DMEG6phqu})_2]\text{Br}$ exhibits better solubility in styrene than the parent complex $[\text{Cu}(\text{DMEGqu})_2]\text{Br}$, it turned out that the new catalyst was completely insoluble in styrene, even at elevated temperatures. Nevertheless, in order to gain information whether $[\text{Cu}(\text{DMEG6phqu})_2]\text{Br}$ could mediate an ATRP, polymerization kinetics were then conducted in solution.

As in earlier studies,^[2] polymerizations were performed in benzonitrile (PhCN) as solvent, since it provides high polarity, good miscibility with styrene, a high boiling point, and it is rather non-hazardous. Polymerizations were conducted at 110 °C and with EBrib as initiator. Complexes were generated in situ in the polymerization mixture (copper salt to ligand ratio: 1/2; for details about the polymerization, see Experimental Section). Conversion was measured by ^1H -NMR spectroscopy, the molecular mass distribution was determined by gel permeation chromatography (GPC). Figure 6 shows a semilogarithmic plot of conversion vs. time. In Figure 7, the molar mass development vs. conversion is depicted. Polymerizations were performed at least three times and the graphs show averaged data. By means of kinetic studies, it was already proven that bischelate Cu^{I} species exclusively catalyse the ATRP.^[2]

An ATRP proceeds with pseudo-first-order kinetics. The concentration of active radical species is rather low and thus termination reactions are effectively suppressed. Under these conditions, the concentration of polymerizing chains stays constant and the polymerization rate only depends on the monomer concentration. Linearity of the semilogarithmic conversion plot (Figure 6) indicates a controlled polymerization and thus a controlled ATRP. The M_n/PD vs. conversion plot (Figure 7) provides additional information about the polymerization.

Values for M_n are only available for polymer samples with a conversion higher than 20%, since polymers with smaller

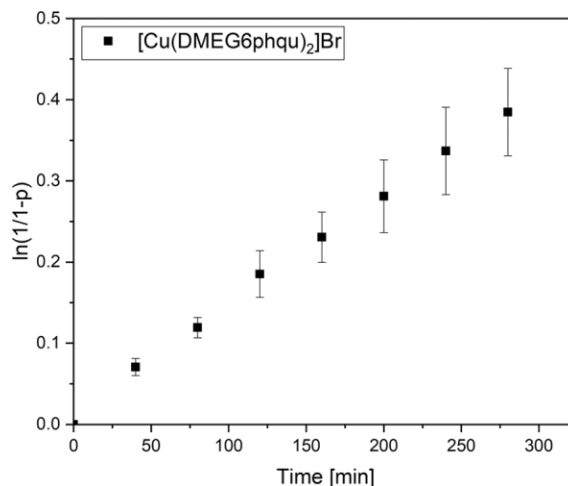


Figure 6. Semilogarithmic kinetic plot for a styrene polymerization in solution (PhCN) mediated by $[\text{Cu}(\text{DMEG6phqu})_2]\text{Br}$. Conditions: 110 °C; ratio: monomer (styrene)/catalyst/ initiator (EBrib) = 100/1/1.

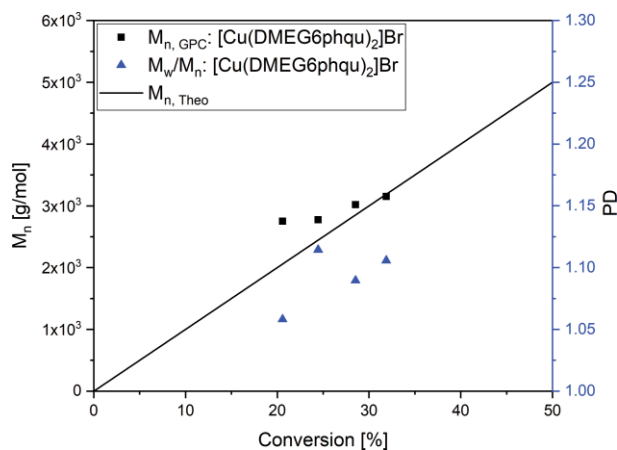


Figure 7. M_n/PD vs. conversion for styrene polymerizations in solution (PhCN) mediated by $[\text{Cu}(\text{DMEG6phqu})_2]\text{Br}$. Conditions: 110 °C; ratio: monomer (styrene)/catalyst/initiator (EBrib) = 100/1/1.

molar masses could not be precipitated. The first monitored point exhibits a slightly increased M_n , since the polymer sample did not precipitate homogeneously. $M_{n,\text{GPC}}$ finely follows $M_{n,\text{Theo}}$, indicating a controlled polymerization. The polydispersity provides information about the molecular mass distribution with $\text{PD} = M_w/M_n$. The values of PD are around 1.05–1.10 throughout the course of reaction. This indicates a very narrow molecular mass distribution and high polymerization control.

In a previous study, polymerization kinetics in solution were performed with the parent complex $[\text{Cu}(\text{DMEGqu})_2]\text{Br}$.^[2] Table 5 summarizes k_{obs} of the newly developed catalyst $[\text{Cu}(\text{DMEG6phqu})_2]\text{Br}$ in comparison with k_{obs} of the parent complex.^[2] The new catalyst exhibits a lower value for k_{obs} than $[\text{Cu}(\text{DMEGqu})_2]\text{Br}$. k_{obs} depends on K_{ATRP} and although K_{ATRP} values for both complexes do not significantly differ, polymerizations with $[\text{Cu}(\text{DMEG6phqu})_2]\text{Br}$ proceed significantly slower. It must be considered that besides K_{ATRP} k_{obs} depends on various factors (solubility of the complexes, rate

of termination reactions, *persistent radical effect*). Comparing catalyst activities by means of k_{obs} thus is only possible to a limited extent.^[26] However, it can be stated that $[\text{Cu}(\text{DMEG6phqu})_2]\text{Br}$ is suitable for solution ATRP of styrene and does not largely differ from previous reported systems by means of polymerization velocity and control.

Table 5. k_{obs} for $[\text{Cu}(\text{DMEG6phqu})_2]\text{Br}$ and $[\text{Cu}(\text{DMEGqu})_2]\text{Br}$. Styrene ATRP in PhCN. Conditions: 110 °C. Ratio: M/cat./init. = 100/1/1.

	L = DMEG6phqu	L = DMEGqu ^[2]
$k_{\text{obs}} / \text{s}^{-1}$	$2.5 \pm 0.1 \times 10^{-05}$	$4.2 \pm 0.2 \times 10^{-05}$

Conclusions

Within this study the synthesis of the phenyl-substituted guanidinoquinoline ligand DMEG6phqu was presented. The nitration step of our synthetic approach to C6 substituted GUAqu ligands had to be optimized due to poor solubility of the 4-aminobiphenyl precursor. DMEG6phqu as well as the complexes $[\text{Cu}(\text{DMEG6phqu})\text{Br}]$ and $[\text{Cu}(\text{DMEG6phqu})_2]\text{Br}$ could be crystallized and characterized. Structural properties of the DMEG6phqu ligand did not show significant differences in comparison with known DMEG6Rqu ($R = \text{H}, \text{et}, \text{bu}$) ligands.

In contrast to previously published $\text{Cu}^{\text{I}}\text{Br}$ complexes of DMEG6Rqu ($R = \text{H}, \text{et}$) ligands, $[\text{Cu}(\text{DMEG6phqu})\text{Br}]$ crystallized as a trigonal planar monochelate complex. The $\text{Cu}^{\text{I}}\text{Br}_2$ complex on the other hand strongly resembles previously published Cu^{II} complexes of DMEG6Rqu ($R = \text{H}$ or et) ligands. Since in polymerization catalysis it is of greater interest to know about the complex structure in solution, NMR, UV/Vis, and EPR experiments with complex solutions were performed. Thus, it could be demonstrated that DMEG6phqu forms a bischelate $\text{Cu}^{\text{I}}\text{Br}$ complex in solution. EPR spectra of $[\text{Cu}(\text{DMEG6phqu})_2]\text{Br}$ in solid state as well as in solution indicate that the Cu^{II} complex reveals the same constitution in both solid state and solution.

With respect to ATRP, the redox potential of the activator/deactivator couple was determined. Furthermore, K_{ATRP} was measured and polymerization kinetics were performed. Phenylation of the quinoline backbone has no significant influence on $E_{1/2}$ and K_{ATRP} of the corresponding complexes. Contrary to our expectations, copper bromide complexes of DMEG6phqu turned out to be completely insoluble in styrene, even at elevated temperatures. Thus, ATRP kinetics were performed in solution. $[\text{Cu}(\text{DMEG6phqu})_2]\text{Br}$ mediates in solution a slower ATRP of styrene as $[\text{Cu}(\text{DMEGqu})_2]\text{Br}$.

It appeared that electronics of DMEGqu ligands can only hardly be influenced by backbone substitution. This became already apparent in alkylated DMEG6Rqu ligands and could be confirmed with this work. In following studies, the influence of further electron donating and withdrawing substituents should be evaluated.

Experimental Section

General: Ligand and complex syntheses were performed under inert conditions by using Schlenk techniques and a glove box in a nitrogen atmosphere. Solvents were purified according to the literature and kept under inert conditions.^[27] Chemicals for the synthesis of the ligands as well as $\text{Cu}^{\text{II}}\text{Br}_2$ for complex syntheses were all purchased from ABCR, Grüssing, AppliChem, Acros Organics or TCI and were used as received without further purification. $\text{Cu}^{\text{I}}\text{Br}$ and the Vilsmeier salt N,N' -dimethylethylene-chloroformamidinium chloride (DMEG-VS) were synthesized as described in the literature.^[17,28]

IR Spectroscopy: ATR IR spectra were measured with a Shimadzu IRTracer 100 with CsI beamsplitter in combination with a Specac Quest ATR unit (resolution 2 cm^{-1}).

Mass Spectrometry: EI mass spectra were obtained with a ThermoFisher Scientific Finnigan MAT 95 mass spectrometer. ESI mass spectra were obtained with a ThermoFisher Scientific LTQ Orbitrap XL. The source voltage was 4.49 kV, the capillary temperature amounted to 299.54 °C. The tube lens voltage lay between 110 and 130 V.

Elemental Analysis: Elemental analyses were performed with an Elemental varioEL or Elementar varioEL cube.

NMR Measurements: ^1H - and ^{13}C -NMR spectra were measured with a Bruker Avance III HD 400 or a Bruker Avance II 400 nuclear magnetic resonance spectrometer. Measurements were performed in fully deuterated solvents. The residual signal of the solvent served as an internal standard.

EPR Measurements: X-band electron paramagnetic resonance spectra were measured with a Magnetech Mini Scope MS 400. The EPR setup included a microwave frequency counter Magnetech FC 400 and the Resonator Rectangular TE102. Measurements were performed in Hirschmann micropipettes with a calibrated volume of 50 μL . Details about the chosen measurement parameters are given at the spectra in the SI.

Gel Permeation Chromatography: The average molecular masses and the mass distributions of the obtained polystyrene samples were determined by gel permeation chromatography (GPC) in THF as mobile phase at a flow rate of 1 $\text{mL}\cdot\text{min}^{-1}$. The utilized GPCmax VE-2001 from Viscotek is a combination of an HPLC pump, two Malvern Viscotek T columns (porous styrene divinylbenzene copolymer) with a maximum pore size of 500 and 5000 Å and a refractive index detector (VE-3580) and a viscometer (Viscotek 270 Dual Detector). Universal calibration was applied to evaluate the chromatographic results.

UV/Vis Setup for K_{ATRP} Determination: UV/Vis measurements were performed with an Avantes AvaSpec-ULS2048 CCD-Spectrometer and an Avantes AvaLight-DH-S-BAL lightsource. The measurements were done in Hellma QS screwcap-cuvettes with an optical pathlength of 10.00 mm.

UV/Vis Setup for the Titration Experiment: UV/Vis measurements were performed with an Agilent Technologies Cary 60 UV/Vis spectrophotometer. The spectra were obtained with a quartz glass immersion probe (Helma, 1 mm) connected via a Cary 50 fibre optic coupler. Measurements were performed in a commercial Schlenk measurement cell.

CV Measurements: The measurements were performed at room temperature with a Metrohm Autolab Potentiostat PGSTAT 101 using a three-electrode arrangement with a Pt disc working electrode (1 mm

diameter), a Pt wire as counter electrode and an Ag/AgCl reference electrode. The measurements were performed in CH_3CN / $0.1 \text{ mol}\cdot\text{L}^{-1}$ NBu_4PF_6 with a sample concentration of 10 mM. Ferrocene was added as an internal standard after the measurements of the sample and all potentials are referenced relative to the Fc/Fc^+ couple. Cyclic voltammograms were measured with $200 \text{ mV}\cdot\text{s}^{-1}$, $100 \text{ mV}\cdot\text{s}^{-1}$, $50 \text{ mV}\cdot\text{s}^{-1}$, and $20 \text{ mV}\cdot\text{s}^{-1}$.

X-ray Diffraction Analysis: The single crystal diffraction data for DMEG6phqu, $[\text{Cu}(\text{DMEG6phqu})\text{Br}]$, and $[\text{Cu}(\text{DMEG6phqu})_2\text{Br}]\text{Br}$ are presented in Table 6. The data were collected with a Bruker D8 goniometer with APEX CCD detector. An Incoatec microsource with $\text{Mo-}K_\alpha$ radiation ($\lambda = 0.71073 \text{ \AA}$) was used and temperature control was achieved with an Oxford Cryostream 700. Crystals were mounted with grease on glass fibers and data were collected at 100 K in ω -scan mode. Data were collected with SMART,^[29] integrated with SAINT^[29] and corrected for absorption by multi-scan methods with SADABS.^[29]

The structure was solved by direct and conventional Fourier methods and all non-hydrogen atoms were refined anisotropically with full-matrix least-squares based on F^2 (XPREP,^[30] SHELXS-97,^[31] and ShelXle^[32]). Hydrogen atoms were derived from difference Fourier maps and placed at idealized positions, riding on their parent C atoms, with isotropic displacement parameters $U_{\text{iso}}(\text{H}) = 1.2U_{\text{eq}}(\text{C})$ and $1.5U_{\text{eq}}(\text{C methyl})$. All methyl groups were allowed to rotate but not to tip.

In the complex $[\text{Cu}(\text{DMEG6phqu})_2\text{Br}]\text{Br}$ it was not possible to model the two water molecules in an adequate manner, and the data set was treated with the SQUEEZE routine as implemented in PLATON.^[33,34]

Crystallographic data (excluding structure factors) for the structures in this paper have been deposited with the Cambridge Crystallographic Data Centre, CCDC, 12 Union Road, Cambridge CB21EZ, UK. Copies of the data can be obtained free of charge on quoting

the depository numbers CCDC-1844282 for DMEG6phqu, CCDC-1844283 for $[\text{Cu}(\text{DMEG6phqu})\text{Br}]$, and CCDC-1844284 for $[\text{Cu}(\text{DMEG6phqu})_2\text{Br}]\text{Br}$ (Fax: +44-1223-336-033; E-Mail: deposit@ccdc.cam.ac.uk, http://www.ccdc.cam.ac.uk).

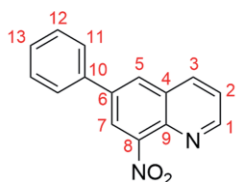
Synthesis of Ligand Precursor 4-Phenyl-2-nitroaniline (NO₂phan):

NO₂phan was synthesized according to various modified literature procedures.^[14–16] 4-Phenylaniline (16.9 g, 100 mmol) was suspended in acetic anhydride (280 mL). The mixture was heated to reflux for 30 min and subsequently cooled to 0 °C. Afterwards, the mixture was carefully poured into iced water (2 L). Thus, 4-phenylacetamide precipitated as a colorless solid. The precipitate was washed with generous amounts of water and dried under high vacuum (1×10^{-3} mbar) overnight. 4-Phenylacetamide (20.9 g, 98.9 mmol, 99%) was isolated. Acetic acid was added to 4-phenylacetamide until it was completely dissolved (300 mL). Afterwards the solution was heated to 70 °C whilst stirring and fuming HNO_3 (99%, 17.2 mL, ex.) in acetic acid (17.2 mL) was carefully added via a dropping funnel. The reaction mixture was heated to 70 °C for 1 h and NO_2 formed during the reaction was quenched by leading it through a washing bottle filled with an aqueous solution of NaOH. The red solution was poured into iced water (1 L). 4-Phenyl-2-nitroacetamide precipitated as a yellow solid, which was filtered off, washed with generous amounts of water and dried under high vacuum (1×10^{-3} mbar). 4-Phenyl-2-nitroacetamide (25.0 g, 97.6 mmol, 98%) was isolated. 4-Phenyl-2-nitroacetamide was dissolved in hot ethanol (125 mL) and an aqueous KOH solution (25 mL, 50%) was carefully added via a dropping funnel. The reaction mixture was heated to reflux for additional 20 min and subsequently cooled to -35 °C. The precipitated red product was recrystallized from ethanol for purification. Red solid. Yield: 7.3 g (34.1 mmol, 34%). **¹H NMR** (400 MHz, CDCl_3): $\delta = 8.39$ (d, $^4J_{\text{HH}} = 2.0$ Hz, 1 H, CH), 7.66 (dd, $^3J_{\text{HH}} = 8.5$, $^4J_{\text{HH}} = 2.3$ Hz, 1 H, CH), 7.57 (m, 2 H, CH), 7.45 (m, 2 H, CH), 7.35 (m, 1 H, CH), 6.91 (d, $^3J_{\text{HH}} = 8.3$ Hz, 2 H, CH), 6.12 (br. s, 2 H, NH_2) ppm; in accordance with literature data.^[35]

Table 6. Crystallographic data and parameters of DMEG6phqu, $[\text{Cu}(\text{DMEG6phqu})\text{Br}]$, and $[\text{Cu}(\text{DMEG6phqu})_2\text{Br}]\text{Br}$.

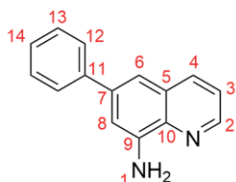
	DMEG6phqu	$[\text{Cu}(\text{DMEG6phqu})\text{Br}]$	$[\text{Cu}(\text{DMEG6phqu})_2\text{Br}]\text{Br}$
Empirical formula	$\text{C}_{20}\text{H}_{20}\text{N}_4$	$\text{C}_{20}\text{H}_{20}\text{BrCuN}_4$	$\text{C}_{40}\text{H}_{40}\text{Br}_2\text{CuN}_8$
Formula mass / $\text{g}\cdot\text{mol}^{-1}$	316.40	459.85	856.16
Crystal size /mm	$0.18 \times 0.17 \times 0.15$	$0.16 \times 0.14 \times 0.13$	$0.15 \times 0.14 \times 0.13$
T /K	100(2)	100(2)	100(2)
Crystal system	monoclinic	monoclinic	monoclinic
Space group	$C2/c$	$P2_1/n$	$P2_1/c$
a / \AA	27.187(8)	12.332(2)	18.6090(13)
b / \AA	7.020(2)	7.7143(12)	16.2503(11)
c / \AA	17.428(5)	19.997(3)	13.6624(9)
α / $^\circ$	90	90	90
β / $^\circ$	104.099(4)	105.100(2)	105.6270(10)
γ / $^\circ$	90	90	90
V / \AA^3	3226.0(16)	1836.8(5)	3978.8(5)
Z	8	4	4
$\rho_{\text{calcd.}}$ / $\text{g}\cdot\text{cm}^{-3}$	1.303	1.663	1.429
μ / mm^{-1}	0.080	3.376	2.596
λ / \AA	0.71073	0.71073	0.71073
$F(000)$	1344	928	1740
hkl range	$-35/35, -9/9, -22/22$	$-17/17, -10/10, -28/28$	$-24/24, -21/21, -18/18$
Reflections collected	20693	27155	55291
Independent reflections	3857	5431	10006
$R_{\text{int.}}$	0.0466	0.0655	0.0897
No. parameters	219	237	464
R_1 [$I \geq 2\sigma(I)$]	0.0432	0.0375	0.0470
wR_2 (all data)	0.1179	0.0987	0.1209
Goodness-of-fit	1.048	1.023	1.043
$\Delta\rho_{\text{fin}}$ max/min / $e\cdot\text{\AA}^{-3}$	0.378/−0.183	0.838/−0.552	1.003/−1.040

Synthesis of Ligand Precursor 6-Phenyl-8-nitroquinoline (NO₂6phqu):



NO₂6phqu was synthesized according to a modified protocol by Wielgosz-Collin et al.^[36] In a 1 L two-necked flask first NO₂phan (6.7 g, 31.2 mmol, 1.0 equiv.) was dissolved in *n*-butanol (30 mL). HCl (conc., 7.5 mL) and *p*-chloranil (7.7 g, 31.2 mmol, 1.0 equiv.) were added. The mixture was heated to reflux and within 2 h acrolein (2.5 g, 43.7 mmol, 1.4 Eq) in *n*-butanol (7.5 mL) was added via a dropping funnel. With the addition of acrolein the reaction mixture changed its color from yellow-brownish to black. The mixture was cooled to room temperature and ZnCl₂ (5.1 g, 37.4 mmol, 1.2 equiv.) in THF (65 mL) was added. Afterwards, the reaction mixture was again heated to reflux for 1 h, then slowly cooled to 0 °C and stirred at that temperature for 2 h. The solid formed was filtered and put on ice. After neutralizing with an aqueous solution of NaOH, the mixture was extracted with dichloromethane (3 × 200 mL). The combined organic layers were dried over MgSO₄ and the solvent removed in vacuo. The crude product was purified by column chromatography (silica gel, 100% dichloromethane → 98% dichloromethane + 2% methanol). Colorless solid. Yield: 4.8 g (19.2 mmol, 62%). ¹H NMR (400 MHz, CDCl₃): δ = 9.07 (dd, ³J_{HH} = 4.1, ⁴J_{HH} = 1.6 Hz, 1 H, CH, 1), 8.32 (m, 2 H, CH, 3, 7), 8.20 (d, ⁴J_{HH} = 2.0 Hz, 1 H, CH, 5), 7.71 (m, 2 H, CH, 11), 7.59 (dd, ³J_{HH} = 8.3, ⁴J_{HH} = 4.3 Hz, 1 H, CH, 2), 7.54 (m, 2 H, CH, 12), 7.47 (m, H, CH, 13) ppm. ¹³C NMR (100 MHz, CDCl₃): δ = 152.4 (CH, 1), 148.5 (C_q, 8), 138.7 (C_q, 9), 138.6 (C_q, 6), 138.0 (C_q, 10), 136.3 (CH, 3), 129.3 (CH, C_q, 4, 12), 129.1 (CH, 5), 128.8 (CH, 13), 127.3 (CH, 11), 123.5 (CH, 7), 123.1 (CH, 2), 28.6 (CH₂, 10), 15.1 (CH₃, 11) ppm. IR (ATR): $\tilde{\nu}$ = 3093 [vw, v(C-H_{arom})], 3073 [w, v(C-H_{arom})], 3055 [w, v(C-H_{arom})], 1596 (w), 1578 (w), 1532 [s, v(N=O)], 1490 (m), 1461 (w), 1441 (w), 1427 (vw), 1402 (w), 1385 (m), 1369 (m), 1356 (s), 1338 (m), 1184 (w), 1132 (w), 1078 (w), 1059 (w), 1024 (w), 1000 (vw), 982 (vw), 969 (w), 945 (vw), 919 (w), 908 (vw), 898 (m), 881 (s), 870 (w), 842 (vw), 799 (m), 796 (m), 774 (s), 758 (s), 748 (vs), 691 (vs), 652 (w), 640 (s), 617 (vw), 575 (m), 535 (w), 527 (w), 500 (m), 447 (m), 410 (vw), 397 (vw), 383 (w), 354 (w), 316 (w), 299 (w), 292 (vw), 283 (w), 278 (w), 273 (w), 266 (m), 253 (m) cm⁻¹. MS (EI⁺-HR): *m/z* calcd. for C₁₅H₁₀O₂N₂ [M]⁺: 250.0737; found: 250.0732. C₁₅H₁₀N₂O₂: calcd. C 71.99, H 4.03, N 11.19%; found: C 72.32, H 3.98, N 11.00%.

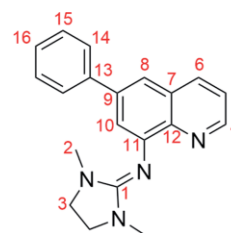
Synthesis of Ligand Precursor 6-Phenyl-8-aminoquinoline (NH₂6phqu):



In an oven dried 500 mL Schlenk-flask first Pd/C (10%Pd basis, 0.5 g, 2.5 mol%) was suspended in MeOH (200 mL). Afterwards, NO₂6phqu (4.8 g, 19.2 mmol, 1 equiv.) was added and the flask was sealed with a rubber septum. The flask was flushed with H₂ and stirred for 24 h at ambient temperature. Afterwards, Pd/C was removed. After washing

the catalyst with additional acetonitrile (150 mL), the organic phases were combined and the solvent removed in vacuo. The crude product was purified by column chromatography (silica gel, ethyl acetate/hexanes: 1/1). Bright yellow solid. Yield: 3.3 g (15.0 mmol, 78%). ¹H NMR (400 MHz, CDCl₃): δ = 8.78 (dd, ³J_{HH} = 4.1, ⁴J_{HH} = 1.6 Hz, 1 H, CH, 2), 8.11 (dd, ³J_{HH} = 8.3, ⁴J_{HH} = 1.5 Hz, 1 H, CH, 4), 7.71 (m, 2 H, CH, 12), 7.49 (m, 2 H, CH, 13), 7.40 (m, 4 H, CH, 3, 6, 14), 7.21 (d, ⁴J_{HH} = 1.8 Hz, 1 H, CH, 8), 5.08 (br. s, 2 H, NH₂, 1) ppm. ¹³C NMR (100 MHz, CDCl₃): δ = 146.6 (CH, 2), 144.1 (C_q, 9), 141.1 (C_q, 11), 140.1 (C_q, 7), 137.9 (C_q, 10), 136.1 (CH, 4), 128.9 (C_q, 5), 128.7 (CH, 13), 127.4 (CH, 14), 127.3 (CH, 12), 121.7 (CH, 3), 114.2 (CH, 6), 109.6 (CH, 8) ppm. IR (ATR): $\tilde{\nu}$ = 3468 [w, v(N-H)], 3301 [w, v(N-H)], 3171 [w, v(N-H)], 3026 [vw, v(C-H_{arom})], 1622 (m), 1600 (m), 1586 (m), 1577 (m), 1506 (m), 1491 (m), 1459 (w), 1444 (vw), 1422 (m), 1393 (m), 1377 (m), 1342 (w), 1284 (vw), 1248 (w), 1206 (vw), 1156 (w), 1125 (w), 1077 (w), 1033 (w), 1000 (vw), 983 (w), 926 (vw), 870 (w), 859 (m), 847 (s), 797 (w), 789 (vs), 762 (vs), 746 (m), 699 (vs), 663 (m), 658 (m), 590 (m), 570 (w), 536 (w), 517 (w), 506 (m), 501 (m), 463 (w), 423 (w), 418 (w), 412 (m), 397 (m), 387 (m), 358 (m), 354 (m), 349 (m), 324 (m), 321 (w), 309 (m), 304 (m), 283 (w), 279 (m), 266 (m), 253 (w) cm⁻¹. MS (EI⁺-HR): *m/z* calcd. for C₁₅H₁₂N₂ [M]⁺: 220.0995; found: 220.0996. C₁₅H₁₂N₂: calcd. C 81.79, H 5.49, N 12.72%; found: C 81.84, H 5.42, N 12.65%.

Synthesis of Ligand N-(6-Phenylquinolin-8-yl)-1,3-dimethylimidazolidin-2-imine (DMEG6phqu):

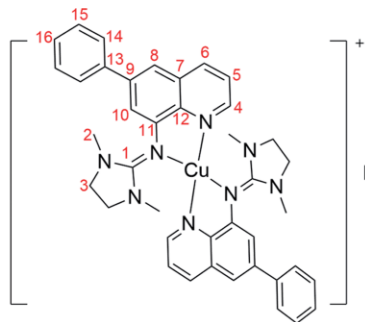


DMEG6phqu was synthesized analogously to the literature using the amine described above.^[37] NH₂6phqu (3.3 g, 15.0 mmol, 1.0 equiv.) was weighed into an oven dried two-necked Schlenk flask and dissolved in acetonitrile (12.5 mL). After addition of triethylamine (3.0 g, 30.0 mmol, 2.0 equiv.), DMEG Vilsmeier salt (2.8 g, 16.5 mmol, 1.1 equiv.) in MeCN (10 mL) was added via a dropping funnel whilst stirring within 15 min. The formation of a colorless solid was observed. The reaction mixture was heated to reflux for 3 h and subsequently a solution of NaOH (40 mmol, 2.03 g, 1.0 equiv.) in water (20 mL) was added. With the addition of the NaOH solution the colorless solid immediately vanished. After removal of the solvent in vacuo, an aqueous KOH solution (30 mL, 50%) was added and the mixture stirred for 2 h. The mixture was extracted with acetonitrile (3 × 50 mL). The combined organic layers were stirred over MgSO₄ and activated charcoal. After filtration, the solvent was removed in vacuo. Remaining urea was removed under high vacuum (1 × 10⁻³ mbar) at 100 °C. The ligand was purified by recrystallization from acetonitrile. Yellow blocky crystals. Yield: 3.8 g (12.0 mmol, 80%). ¹H NMR (400 MHz, CDCl₃): δ = 8.80 (dd, ³J_{HH} = 4.1, ⁴J_{HH} = 1.6 Hz, 1 H, CH, 4), 8.10 (dd, ³J_{HH} = 8.3, ⁴J_{HH} = 1.8 Hz, 1 H, CH, 6), 7.70 (m, 3 H, CH, 5, 14), 7.59 (d, ⁴J_{HH} = 2.0 Hz, CH, 8), 7.42 (m, 2 H, CH, 15), 7.33 (m, 2 H, CH, 10, 16), 3.44 (s, 4 H, CH₂, 3), 2.69 (s, 6 H, CH₂, 2) ppm. ¹³C NMR (100 MHz, CDCl₃): δ = 157.1 (C_{GUA}, 1), 148.9 (CH, 4), 144.2 (C_q, 11), 142.2 (C_q, 12), 140.5 (C_q, 13), 139.5 (C_q, 9), 136.3 (C_q, 6), 129.2 (C_q, 7), 128.8 (CH, 15), 127.5 (CH, 16), 127.4 (CH, 14), 121.3 (CH, 5), 120.8 (CH, 10), 118.8 (CH, 8), 48.4 (CH₂, 3), 34.8 (CH₃, 2) ppm. IR (ATR): $\tilde{\nu}$ = 3040 [w, v(C-H_{arom})],

2936 [w, v(C-H_{aliph})], 2860 [w, v(C-H_{aliph})], 1616 [vs, v(C=N_{gua})], 1603 [vs, v(C=N_{gua})], 1576 (m), 1559 (m), 1479 (vs), 1442 (m), 1417 (m), 1379 (s), 1339 (w), 1281 (m), 1239 (m), 1231 (m), 1200 (w), 1137 (w), 1098 (w), 1076 (w), 1026 (m), 968 (m), 915 (w), 881 (w), 867 (m), 791 (m), 763 (s), 733 (w), 697 (s), 642 (m), 631 (m), 617 (m), 600 (m), 589 (m), 569 (m), 463 (m), 444 (m), 354 (m), 349 (m), 328 (m), 324 (m), 283 (m) cm⁻¹. **MS** (EI⁺-HR): *m/z* calcd. for C₂₀H₂₀N₄ [M]⁺: 316.1684; found: 316.1682. C₂₀H₂₀N₄: calcd. C 75.92, H 6.73, N 17.71%; found: C 74.80, H 6.24, N 17.42%.

Synthesis of [Cu(DMEG6phqu)Br]: To a warm solution of DMEG6phqu (379.7 mg, 1.2 mmol, 2.4 equiv.) in acetonitrile (10 mL), Cu^IBr (71.7 mg, 0.5 mmol, 1.0 equiv.) was added in small portions whilst stirring. A change of color from pale yellow to dark red was observed. Diffusion of diethyl ether led to crystals suitable for X-ray diffraction within 3 d. Bright orange crystals. Yield: 74.0 mg (0.1 mmol, 20%). **IR** (ATR): $\tilde{\nu}$ = 3048 [vw, v(C-H_{arom})], 2927 [vw, v(C-H_{aliph})], 2886 [vw, v(C-H_{aliph})], 2861 [w, v(C-H_{aliph})], 1586 (m), 1575 (m), 1554 [vs, v(C=N_{gua})], 1532 [vs, v(C=N_{gua})], 1485 (s), 1475 (s), 1452 (m), 1441 (m), 1412 (vs), 1389 (s), 1371 (m), 1338 (m), 1298 (m), 1285 (m), 1234 (m), 1187 (w), 1176 (w), 1151 (m), 1139 (w), 1113 (w), 1071 (w), 1042 (w), 1021 (m), 998 (w), 984 (w), 973 (m), 932 (w), 920 (w), 886 (w), 872 (m), 856 (s), 814 (w), 800 (m), 787 (s), 768 (s), 719 (m), 702 (vs), 664 (m), 655 (w), 627 (m), 614 (m), 608 (m), 570 (m), 547 (m), 518 (m), 466 (w), 452 (w), 335 (m), 289 (m), 267 (m), 265 (m) cm⁻¹. **MS** (ESI⁺-HR)[*m/z*]: Isotopic distribution calcd. for C₂₀H₂₀CuBrN₄ [Cu(DMEG6phqu)Br]⁺: 458.0167 (70) [C₂₀H₂₀⁶³Cu⁷⁹BrN₄]⁺, 459.0192 (16) [C₁₉¹³CH₂₀⁶³Cu⁷⁹BrN₄], 460.0150 (100) [C₂₀H₂₀⁶³Cu⁸¹BrN₄] and [C₂₀H₂₀⁶⁵Cu⁷⁹BrN₄], 461.0179 (24) [C₁₉¹³CH₂₀⁶³Cu⁸¹BrN₄] and [C₁₉¹³CH₂₀⁶⁵Cu⁷⁹BrN₄], 462.0135 (33) [C₂₀H₂₀⁶⁵Cu⁸¹BrN₄], 463.0156 (7) [C₁₉¹³CH₂₀⁶⁵Cu⁸¹BrN₄], 464.0191 (1) [C₁₈¹³C₂H₂₀⁶⁵Cu⁸¹BrN₄]; found: 458.0148 (70), 459.0181 (15), 460.0126 (100), 461.0159 (20), 462.0108 (30), 463.0137 (5), 464.0172 (1). C₂₀H₂₀BrCuN₄: calcd. C 52.24, H 4.38, N 12.18%; found: C 52.11, H 4.23, N 12.18%.

Synthesis of [Cu(DMEG6phqu)₂]Br:



DMEG6phqu (22.1 mg, 0.070 mmol, 2 equiv.) and Cu^IBr (5.0 mg, 0.035 mmol, 1 equiv.) were dissolved in [D₃]MeCN whilst stirring. Formation of the complex was affiliated with dark red coloring of the solution. The solution was subjected to NMR and MS spectroscopy. **¹H NMR** (400 MHz, CDCl₃): δ = 8.59 (dd, ³J_{HH} = 4.5, ⁴J_{HH} = 1.5 Hz, 2 H, CH, 4), 8.38 (dd, ³J_{HH} = 8.3, ⁴J_{HH} = 1.5 Hz, 2 H, CH, 6), 7.77 (m, 4 H, CH, 14), 7.65 (d, ⁴J_{HH} = 1.8 Hz, 2 H, CH, 8), 7.52 (m, 5 H, CH, 5, 15), 7.43 (m, 2 H, CH, 10, 16), 3.44 (s, 4 H, CH₂, 3), 2.69 (s, 6 H, CH₂, 2) ppm. **¹³C NMR** (100 MHz, CDCl₃): δ = 163.2 (C_{GUA}, 1), 148.1 (CH, 4), 147.4 (C_q, 12), 141.6 (C_q, 9), 141.1 (C_q, 13), 137.9 (C_q, 6), 131.1 (C_q, 7), 130.0 (CH, 15), 129.0 (CH, 16), 128.4 (CH, 14), 123.8 (CH, 5), 118.0 (CH, 10), 116.6 (CH, 8), 49.1 (CH₂, 3), 35.7 (CH₃, 2) ppm. **MS** (ESI⁺-HR)[*m/z*]: Isotopic distribution calcd. for

C₄₀H₄₀CuN₈ [Cu(DMEG6phqu)₂]⁺: 695.2668 (100) [C₄₀H₄₀⁶³CuN₈]⁺, 696.2703 (48) [C₃₉¹³CH₄₀⁶³CuN₈]⁺, 697.2662 (56) [C₄₀H₄₀⁶⁵CuN₈]⁺, 698.2688 (23) [C₃₉¹³CH₄₀⁶⁵CuN₈]⁺, 699.2720 (5) [C₃₈¹³C₂H₄₀⁶⁵CuN₈]⁺, 700.2738 (1) [C₃₇¹³C₃H₄₀⁶⁵CuN₈]⁺; found: 695.2650 (100), 696.2681 (42), 697.2640 (44), 698.2663 (20), 699.2699 (4), 700.2749 (1). Isotopic distribution calcd. for C₂₀H₂₀CuBrN₄ [Cu(DMEG6phqu)Br]⁺: 458.0167 (70) [C₂₀H₂₀⁶³Cu⁷⁹BrN₄]⁺, 459.0192 (16) [C₁₉¹³CH₂₀⁶³Cu⁷⁹BrN₄], 460.0150 (100) [C₂₀H₂₀⁶³Cu⁸¹BrN₄] and [C₂₀H₂₀⁶⁵Cu⁷⁹BrN₄], 461.0179 (24) [C₁₉¹³CH₂₀⁶³Cu⁸¹BrN₄] and [C₁₉¹³CH₂₀⁶⁵Cu⁷⁹BrN₄], 462.0135 (33) [C₂₀H₂₀⁶⁵Cu⁸¹BrN₄], 463.0156 (7) [C₁₉¹³CH₂₀⁶⁵Cu⁸¹BrN₄], 464.0191 (1) [C₁₈¹³C₂H₂₀⁶⁵Cu⁸¹BrN₄]; found: 458.0148 (70), 459.0181 (15), 460.0126 (100), 461.0159 (20), 462.0108 (30), 463.0137 (5), 464.0172 (1).

Synthesis of [Cu(DMEG6phqu)₂]Br: To a warm solution of DMEG6phqu (379.7 mg, 1.2 mmol, 2.4 equiv.) in 10 mL acetonitrile Cu^{II}Br₂ (111.7 mg, 0.50 mmol, 1.0 equiv.) was added in small portions whilst stirring. A change of color from pale yellow to dark red was observed. Diffusion of diethyl ether led to crystals suitable for X-ray diffraction within one week. Dark red crystals. Yield: 34.4 mg (0.05 mmol, 10%). **IR** (ATR): $\tilde{\nu}$ = 3043 [vw, v(C-H_{arom})], 2946 [vw, v(C-H_{aliph})], 2919 [vw, v(C-H_{aliph})], 2887 [w, v(C-H_{aliph})], 2871 [vw, v(C-H_{aliph})], 1543 [vs, v(C=N_{gua})], 1490 (s), 1469 (m), 1458 (m), 1414 (s), 1393 (vs), 1374 (m), 1341 (m), 1297 (m), 1245 (m), 1232 (m), 1213 (w), 1140 (vw), 1118 (w), 1088 (w), 1045 (w), 1023 (m), 1003 (w), 973 (m), 939 (vw), 912 (vw), 873 (m), 838 (w), 827 (w), 804 (w), 793 (w), 778 (m), 767 (s), 725 (vw), 706 (w), 694 (m), 665 (m), 654 (w), 625 (w), 618 (w), 610 (w), 601 (w), 576 (w), 571 (w), 553 (w), 517 (w), 509 (vw), 461 (w), 450 (w), 354 (w), 350 (m) cm⁻¹. **MS** (ESI⁺-HR)[*m/z*]: Isotopic distribution calcd. for [Cu(DMEG6phqu)₂]Br⁺: 774.1848 (65) [C₄₀H₄₀⁶³Cu⁷⁹BrN₈]⁺, 775.1881 (31) [C₃₉¹³CH₄₀⁶³Cu⁷⁹BrN₈]⁺, 776.1846 (100) [C₄₀H₄₀⁶³Cu⁸¹BrN₈]⁺ and [C₄₀H₄₀⁶⁵Cu⁷⁹BrN₈]⁺, 777.1872 (45) [C₃₉¹³CH₄₀⁶³Cu⁸¹BrN₈]⁺ and [C₃₉¹³CH₄₀⁶⁵Cu⁷⁹BrN₈]⁺, 778.1835 (39) [C₄₀H₄₀⁶⁵Cu⁸¹BrN₈]⁺, 779.1857 (15) [C₃₉¹³CH₄₀⁶⁵Cu⁸¹BrN₈]⁺, 780.1887 (3) [C₃₈¹³C₂H₄₀⁶⁵Cu⁸¹BrN₈]⁺, 781.1900 (1) [C₃₇¹³C₃H₄₀⁶⁵Cu⁸¹BrN₈]⁺; found: 774.1846 (70), 775.1873 (30), 776.1821 (100), 777.1845 (45), 778.1811 (38), 779.1826 (14), 780.1856 (4), 781.1903 (1). Isotopic distribution calcd. for [Cu(DMEG6phqu)₂]Br⁺: 458.0167 (70) [C₂₀H₂₀⁶³Cu⁷⁹BrN₄]⁺, 459.0192 (16) [C₁₉¹³CH₂₀⁶³Cu⁷⁹BrN₄], 460.0150 (100) [C₂₀H₂₀⁶³Cu⁸¹BrN₄] and [C₂₀H₂₀⁶⁵Cu⁷⁹BrN₄], 461.0179 (24) [C₁₉¹³CH₂₀⁶³Cu⁸¹BrN₄] and [C₁₉¹³CH₂₀⁶⁵Cu⁷⁹BrN₄], 462.0135 (33) [C₂₀H₂₀⁶⁵Cu⁸¹BrN₄], 463.0156 (7) [C₁₉¹³CH₂₀⁶⁵Cu⁸¹BrN₄], 464.0191 (1) [C₁₈¹³C₂H₂₀⁶⁵Cu⁸¹BrN₄]; found: 458.0159 (70), 459.0191 (15), 460.0135 (100), 461.0161 (20), 462.0115 (30), 463.0144 (4), 464.0174 (1). C₄₀H₄₀Br₂CuN₈: calcd. C 56.12, H 4.71, N 13.09%; found: C 55.73, H 4.69, N 12.85%.

Polymerization Procedure: Styrene (Acros Organics, 99% stab.), benzonitrile (PhCN, AlzChem), and the initiator ethyl α -bromoisobutyrate (EBrib, abcr, 98%) were freshly distilled over CaH₂. All polymerizations were performed with in situ generated catalysts. First, the copper salt (0.19 mmol, Cu^IBr: 27 mg) next the ligand (0.38 mmol, DMEG6phqu: 120 mg) were directly weighed into the polymerization vessel under inert conditions inside a glovebox. Outside the glove box the prepared Schlenk tube was connected to a Schlenk line. Styrene (19 mmol, 2.2 mL), solvent (PhCN, 1.0 mL), and finally the initiator (0.19 mmol, EBrib: 28 μ L) were added with gastight glass syringes.

After addition of the initiator, the mixture was heated (110 °C) under vigorous stirring. The first sample was taken with a glass pipette under inert conditions after 2.5 min. At this point of time the polymerization

mixture reached its desired temperature and thus was chosen to be starting point of the polymerization. Further samples were taken in certain time intervals. The samples were mixed with CDCl_3 and the conversion measured by $^1\text{H-NMR}$ spectroscopy. Afterwards the polymer was precipitated in ethanol to remove the copper compound and residual monomer. The solid, colorless polystyrene was dried overnight and molecular mass distributions were determined by GPC.

K_{ATRP} Determination: All measurements were performed in oxygen free acetonitrile at 22°C . The acetonitrile was degassed by three freeze-pump-thaw cycles. Stock solutions of the complexes and the cuvettes were prepared in a glovebox under inert conditions.

The stock solutions of the initiator [147 μL (1.00 mmol) EBrib in 10 mL of acetonitrile] and the complexes [0.05 mmol $\text{Cu}^{\text{I}}\text{Br}$ (7.2 mg) and 0.1 mmol ligand (DMEG6phqu: 31.6 mg) in 2 mL of acetonitrile] were prepared. A screwcap cuvette containing a stirring bar was filled with 1.5 mL of acetonitrile and tightly sealed with a silicon septum. A reference spectrum (MeCN) was measured. After addition of 400 μL catalyst solution the time-dependent UV/Vis measurement was started. By adding 100 μL of EBrib solution the reaction was initiated and the formation of the Cu^{II} species was followed by UV/Vis spectroscopy.

Supporting Information (see footnote on the first page of this article): ESR spectra of $\text{Cu}(\text{II})$ complexes, plot for K_{ATRP} determination, UV/Vis spectrum of $[\text{Cu}(\text{DMEG6phqu})_2]\text{Br}$ after addition of excess ligand, NMR spectra of all compounds, VT-NMR spectra of $[\text{Cu}(\text{DMEG6phqu})_2]\text{Br}$.

Acknowledgements

Financial support by the Fonds der Chemischen Industrie (Fonds fellowships for T.R.) is gratefully acknowledged.

Keywords: Atom transfer radical polymerization (ATRP); Copper; Substitution; Guanidine; Quinoline; Molecular structure

References

- a) M. Kato, M. Kamigaito, M. Sawamoto, T. Higashimura, *Macromolecules* **1995**, *28*, 1721–1723; b) J.-S. Wang, K. Matyjaszewski, *Macromolecules* **1995**, *28*, 7901–7910; c) V. Percec, B. Barboiu, *Macromolecules* **1995**, *28*, 7970–7972; d) K. Matyjaszewski, *Macromolecules* **2012**, *45*, 4015–4039.
- T. Rösener, O. Bienemann, K. Sigl, N. Schopp, F. Schnitter, U. Flörke, A. Hoffmann, A. Döring, D. Kuckling, S. Herres-Pawlis, *Chem. Eur. J.* **2016**, *22*, 13550–13562.
- T. Rösener, A. Hoffmann, S. Herres-Pawlis, *Eur. J. Inorg. Chem.* **2018**, *27*, 3164–3175.
- a) K. Min, H. Gao, K. Matyjaszewski, *J. Am. Chem. Soc.* **2005**, *127*, 3825–3830; b) W. Jakubowski, K. Matyjaszewski, *Angew. Chem. Int. Ed.* **2006**, *45*, 4482–4486; *Angew. Chem.* **2006**, *118*, 4594–4598; c) A. J. D. Magenau, N. C. Strandwitz, A. Gennaro, K. Matyjaszewski, *Science* **2011**, *332*, 81–84; d) N. Bortolamei, A. A. Isse, A. J. D. Magenau, A. Gennaro, K. Matyjaszewski, *Angew. Chem. Int. Ed.* **2011**, *50*, 11391–11394; *Angew. Chem.* **2011**, *123*, 11593–11596.
- W. Tang, K. Matyjaszewski, *Macromolecules* **2006**, *39*, 4953–4959.
- A. J. D. Magenau, Y. Kwak, K. Schröder, K. Matyjaszewski, *ACS Macro Lett.* **2012**, *1*, 508–512.
- T. G. Ribelli, M. Fantin, J.-C. Daran, K. F. Augustine, R. Poli, K. Matyjaszewski, *J. Am. Chem. Soc.* **2018**, *140*, 1525–1534.
- a) A. Metz, R. Plothe, B. Glowacki, A. Koszalkowski, M. Scheckenbach, A. Beringer, T. Rösener, J. Michaelis de Vasconcellos, R. Haase, U. Flörke, A. Hoffmann, S. Herres-Pawlis, *Eur. J. Inorg. Chem.* **2016**, *2016*, 4974–4987; b) P. M. Schäfer, M. Fuchs, A. Ohligschläger, R. Rittinghaus, P. McKeown, E. Akin, M. Schmidt, A. Hoffmann, M. A. Liauw, M. D. Jones, S. Herres-Pawlis, *ChemSusChem* **2017**, *10*, 3547–3556; c) N. G. Sedush, V. V. Izraylit, A. K. Mailyan, D. V. Savinov, Y. I. Kiryukhin, S. N. Chvalun, *Mendeleev Commun.* **2017**, *27*, 281–282.
- a) F. Strassl, B. Grimm-Lebsanft, D. Rukser, F. Biebl, M. Biednov, C. Brett, R. Timmermann, F. Metz, A. Hoffmann, M. Rübhausen, S. Herres-Pawlis, *Eur. J. Inorg. Chem.* **2017**, *2017*, 3350–3359; b) S. Herres-Pawlis, S. Binder, A. Eich, R. Haase, B. Schulz, G. Wellenreuther, G. Henkel, M. Rübhausen, W. Meyer-Klaucke, *Chem. Eur. J.* **2009**, *15*, 8678–8682; c) M. Schatz, V. Raab, S. P. Foxon, G. Brehm, S. Schneider, M. Reiher, M. C. Holthausen, J. Sundermeyer, S. Schindler, *Angew. Chem. Int. Ed.* **2004**, *43*, 4360–4363; *Angew. Chem.* **2004**, *116*, 4460–4464; d) C. Würtele, E. Gaoutchenova, K. Harms, M. C. Holthausen, J. Sundermeyer, S. Schindler, *Angew. Chem. Int. Ed.* **2006**, *45*, 3867–3869; *Angew. Chem.* **2006**, *118*, 3951–3954; e) D. Maiti, D.-H. Lee, K. Gaoutchenova, C. Würtele, M. C. Holthausen, A. A. Narducci Sarjeant, J. Sundermeyer, S. Schindler, K. D. Karlin, *Angew. Chem. Int. Ed.* **2008**, *47*, 82–85; *Angew. Chem.* **2008**, *120*, 88–91.
- a) A. Hoffmann, O. Bienemann, I. dos Santos Vieira, S. Herres-Pawlis, *Polymers* **2014**, *6*, 995–1007; b) O. Bienemann, A.-K. Froin, I. dos Santos Vieira, R. Wortmann, A. Hoffmann, S. Herres-Pawlis, *Z. Anorg. Allg. Chem.* **2012**, *638*, 1683–1690; c) A. Hoffmann, O. Bienemann, I. dos Santos Vieira, S. Herres-Pawlis, *Z. Naturforsch. B* **2014**, *69*, 589–595; d) O. Bienemann, R. Haase, A. Jesser, T. Beschnitt, A. Döring, D. Kuckling, I. dos Santos Vieira, U. Flörke, S. Herres-Pawlis, *Eur. J. Inorg. Chem.* **2011**, *2011*, 2367–2379; e) S. H. Oakley, M. P. Coles, P. B. Hitchcock, *Inorg. Chem.* **2003**, *42*, 3154–3156; f) A. S. Brar, S. Kaur, *J. Polym. Sci. A: Polym. Chem.* **2005**, *43*, 5906–5922; g) O. Bienemann, R. Haase, U. Flörke, A. Döring, D. Kuckling, S. Herres-Pawlis, *Z. Naturforsch. B* **2010**, *65*, 798–806.
- B. Dicke, A. Hoffmann, J. Stanek, M. S. Rapp, B. Grimm-Lebsanft, F. Biebl, D. Rukser, B. Maerz, D. Görries, M. Naumova, M. Biednov, G. Neuber, A. Wetzel, S. M. Hofmann, P. Roedig, A. Meents, J. Bielecki, J. Andreasson, K. R. Beyerlein, H. N. Chapman, C. Bressler, W. Zinth, M. Rübhausen, S. Herres-Pawlis, *Nat. Chem.* **2018**, *10*, 355–362.
- J. Stanek, N. Sackers, F. Fink, M. Paul, L. Peters, R. Grunzke, A. Hoffmann, S. Herres-Pawlis, *Chem. Eur. J.* **2017**, *23*, 15738–15745.
- A. Hoffmann, J. Stanek, B. Dicke, L. Peters, B. Grimm-Lebsanft, A. Wetzel, A. Jesser, M. Bauer, M. Gnida, W. Meyer-Klaucke, M. Rübhausen, S. Herres-Pawlis, *Eur. J. Inorg. Chem.* **2016**, *2016*, 4731–4743.
- D. T. Glatzhofer, R. R. Roy, K. N. Cossey, *Org. Lett.* **2002**, *4*, 2349–2352.
- E. Berliner, B. Newman, T. M. Riaboff, *J. Am. Chem. Soc.* **1955**, *77*, 478–480.
- C. Dell’Erba, G. Garbarino, G. Guanti, *Tetrahedron* **1971**, *27*, 113–121.
- W. Kantlehner, E. Haug, W. W. Mergen, P. Speh, T. Maier, J. J. Kapassakalidis, H.-J. Bräuner, H. Hagen, *Liebigs Ann. Chem.* **1984**, *1984*, 108–126.
- S. Herres-Pawlis, U. Flörke, G. Henkel, *Eur. J. Inorg. Chem.* **2005**, *2005*, 3815–3824.
- J. Börner, I. dos Santos Vieira, U. Flörke, A. Döring, D. Kuckling, S. Herres-Pawlis, in *Renewable and Sustainable Polymers, ACS Symposium Series*, vol. 1063 (Eds.: G. F. Payne, P. B. Smith), American Chemical Society, Washington DC, **2011**, pp. 169–200.
- V. Raab, K. Harms, J. Sundermeyer, B. Kovacevic, Z. B. Maksic, *J. Org. Chem.* **2003**, *68*, 8790–8797.
- A. W. Addison, T. N. Rao, J. Reedijk, J. van Rijn, G. C. Verschoor, *J. Chem. Soc., Dalton Trans.* **1984**, 1349.

- [22] I. Shimizu, Y. Morimoto, D. Faltermeier, M. Kerscher, S. Paria, T. Abe, H. Sugimoto, N. Fujieda, K. Asano, T. Suzuki, P. Comba, S. Itoh, *Inorg. Chem.* **2017**, *56*, 9634–9645.
- [23] W. A. Braunecker, N. V. Tsarevsky, A. Gennaro, K. Matyjaszewski, *Macromolecules* **2009**, *42*, 6348–6360.
- [24] N. G. Connelly, W. E. Geiger, *Chem. Rev.* **1996**, *96*, 877–910.
- [25] W. Tang, N. V. Tsarevsky, K. Matyjaszewski, *J. Am. Chem. Soc.* **2006**, *128*, 1598–1604.
- [26] K. Matyjaszewski, B. Göbelt, H.-j. Paik, C. P. Horwitz, *Macromolecules* **2001**, *34*, 430–440.
- [27] A. J. Niestroj, M. E. Maier, *Praxis in der Organischen Chemie*; VCH, Weinheim, **1997**.
- [28] H.-D. Hardt, *Z. Anorg. Allg. Chem.* **1959**, *301*, 87–96.
- [29] Bruker, SMART (Version 5.631), SAINT (Version 8.37A) and SADABS (Version 2008/1); AXS Inc, Madison, Wisconsin, USA, **2008**.
- [30] Bruker, *XPREP Vers 5.1/NT*; AXS Inc, Madison, Wisconsin, USA, **2007**.
- [31] G. M. Sheldrick, *Acta Crystallogr., Sect. A* **1990**, *46*, 467–473.
- [32] C. B. Hübschle, G. M. Sheldrick, B. Dittrich, *J. Appl. Crystallogr.* **2011**, *44*, 1281–1284.
- [33] A. L. Spek, *PLATON, A Multipurpose Crystallographic Tool*, Utrecht University, Utrecht (The Netherlands), **2008**.
- [34] A. L. Spek, *Acta Crystallogr., Sect. D* **2009**, *65*, 148–155.
- [35] P. S. Charifson, A.-L. Grillo, T. H. Grossman, J. D. Parsons, M. Badia, S. Bellon, D. D. Deininger, J. E. Drumm, C. H. Gross, A. LeTiran, Y. Liao, N. Mani, D. P. Nicolau, E. Perola, S. Ronkin, D. Shannon, L. L. Swenson, Q. Tang, P. R. Tessier, S.-K. Tian, M. Trudeau, T. Wang, Y. Wei, H. Zhang, D. Stamos, *J. Med. Chem.* **2008**, *51*, 5243–5263.
- [36] G. Wielgosz-Collin, M. Duflos, P. Pinson, G. Le Baut, P. Renard, C. Bennejean, J. Boutin, M. Boulanger, *J. Enzymatic Inhib. Med. Chem.* **2002**, *17*, 449–453.
- [37] A. Hoffmann, J. Börner, U. Flörke, S. Herres-Pawlis, *Inorg. Chim. Acta* **2009**, *362*, 1185–1193.

Received: June 16, 2018

Published online: August 17, 2018